Structural Characterization of Cationic Liposomes Loaded with Sugar-Based Carboranes

Sandra Ristori,* Julian Oberdisse,† Isabelle Grillo,‡ Alessandro Donati,§ and Olivier Spalla‖
*Department of Chemistry, Università di Firenze, Sesto Fiorentino, Italy; †Groupe de Dynamique des Phases Condensées, Université de Montpellier II, Montpellier, France; ‡Institut Laue Langevin, Grenoble, France; §Department of Chemical and Biosystem Sciences, Università di Siena, Siena, Italy; and ‖DRECAM/SCM, Lions, Commissariat à l'Énergie Atomique, Saclay, Gif sur Yvette, France

ABSTRACT In this article we report the physicochemical characterization of cationic liposomes loaded with orthocarborane and two of its sugar-containing derivatives. Carboranes are efficient boron delivery agents in boron neutron capture therapy, an anticancer treatment based on neutron absorption by ^{10}B nuclei. Cationic liposomes were prepared using the positively charged DOTAP and the zwitterionic DOPE, as a helper lipid. These liposomes are currently used in gene therapy for their ability in targeting the cell nucleus; therefore they can be considered appropriate vectors for boron neutron capture therapy, in the quest of reducing the high boron amount that is necessary for successful cancer treatment. Boron uptake was determined by an original in situ method, based on neutron absorption. The structural properties of the loaded liposomes were studied in detail by the combined use of small angle x-ray scattering and small angle neutron scattering. These techniques established the global shape and size of liposomes and their bilayer composition. The results were discussed in term of molecular properties of the hosted drugs. Differences found in the insertion modality were correlated with the preparation procedure or with the specific shape and lipophilic-hydrophilic balance of each carborane.

INTRODUCTION

Boron neutron capture therapy (BNCT) is a two-step cancer treatment (Larsson et al., 1997; Hawthorne et al., 2001; Soloway et al., 1998; Barth, 2003), especially suited for radio-resistant and highly invasive tumors. It is based on boron accumulation into neoplastic cells and subsequent irradiation of patients with a thermal or epithermal neutron beam. Natural isotopic composition of boron is 20% ^{10}B and 80% ^{11}B. Of these two species, ^{10}B has by far the larger absorption cross section for neutrons, so that the relevant fission process taking place in BNCT can be written as (Sjöland et al., 1997)

$$^{10}B + n \rightarrow {}^{7}Li + {}^{4}He + \gamma. \quad (1)$$

Heavy particle release induces cell damage and death, but this effect is mainly limited to those cells where boron is located, since the penetration length of ^{7}Li and ^{4}He in tissues does not exceed 5–10 μm. Delivery of a large number of boron atoms plays a key role for the success of BNCT and it has been estimated that $\sim 10^9$ nuclei of ^{10}B have to be located inside each tumor cell for the therapy to be effective (Fairchild and Bond, 1985). If boron delivery takes place in the cell nucleus, the number of required ^{10}B nuclei is at least one order-of-magnitude lower (Ryynänen et al., 2000; Braun et al., 2003). Still, huge amounts of boron are needed and much effort is currently being focused on finding appropriate carriers.

Liposomes are generally recognized as efficient, nontoxic drug vectors, able to concentrate the active molecules at delivery sites (Lasic and Papahadjopoulus, 1998). In the specific case of targeting tumor tissues, it has been demonstrated that liposomes of appropriate size (i.e., $\sim$100 nm mean diameter) can extravasate through their leaky endothelium and penetrate the defective outer membrane of neoplastic cells (Matsumura and Maeda, 1986; Shelly et al., 1992; Nagayasu et al., 1999). In particular, cationic liposomes may act as suitable carriers in BNCT, because they are known to form stable complexes with DNA, and are widely studied as nonviral vectors for gene therapy purposes (Lasic et al., 1997; Miller, 1998; Safinya, 2001).

Carboranyl-glucosydes have been synthesized to be used in BNCT (Tietze and Bothe, 1998; Giovenzana et al., 1999), and preliminary experiments in vitro have shown enhanced uptake by tumor cells (Tietze et al., 2001), with respect to healthy cells. This is probably due to the fact that sugars are among the building units most required by cells proliferating with abnormal rate. These boronated compounds also possess the favorable property, common to all carboranyl-derivatives, to carry 10 boron atoms per molecule, the chemical formula of the carborane unit being $-C_2B_{10}H_{11}$.

In this work, our first aim was to establish if 1,2-dicarbadodecaborane, made by the icosahedral carborane cage, and two of its sugar derivatives (i.e., the glucosyl and lactosyl functionalized compounds), could be efficiently incorporated into cationic liposomes. To the best of our knowledge, cationic liposomes have not yet been used as carriers for borocompounds in BNCT, notwithstanding their appealing properties. A detailed investigation of the loaded

Submitted July 15, 2004, and accepted for publication October 7, 2004.

Address reprint requests to Dr. Sandra Ristori, Dept. of Chemistry, Via della Lastruccia 3, 50019 Sesto Fiorentino (Firenze), Italy. Tel.: 39-055-457-3048; Fax: 39-055-457-3385; E-mail: ristori@unifi.it.

0006-3495/05/01/535/13 $2.00 doi: 10.1529/biophysj.104.049080

liposome structural features was performed by small angle scattering of x rays (SAXS) and small angle scattering of neutrons (SANS). We found that the insertion of host molecules may have a drastic effect on the organization of the lipids within the bilayer and, consequently, that it can influence the size and shape of liposomes themselves. As mentioned above, both the size of the liposomes, and the possibility of their anchoring to the targeting species in a way that preserves their functionality, are critical requirements for drug delivery into tumor cells. Thus, to obtain the expected biomedical performance, and to avoid many unnecessary trial-and-error tests, the successful tailoring of drug carriers requires extensive physicochemical characterization. In turn, this entails determining the composition, global shape, and internal structure of the boron-loaded vectors.

Small angle scattering techniques are well-established methods for the study of self-assembling structures in a wide range of scale lengths, which is approximately from one nanometer to a few hundred nanometers (Lindner and Zemb, 2002). In particular, the combined use of x rays and neutrons, which rely on different contrast mechanisms, is suited for sugar-containing amphiphiles (Cantù et al., 1998; Zhang et al., 1999; Stradner et al., 2000; Irai et al., 2003). In fact, the polar head's high electron density allows the investigation of the hydrophilic region of the bilayer by x-ray scattering, whereas neutrons are more sensitive to the hydrophobic core (Wiener and White, 1991). From our neutron scattering curves the overall shape and size of liposomes could be calculated as well. Since molecular volumes, layer thicknesses, and scattering length densities are not independent variables (Hayter and Penfold, 1983), the parallel calculation of SAXS and SANS spectra, if performed at the absolute scale, also provides a useful means for obtaining an accurate description of the systems under study (Arleth et al., 1997; Dupuy et al., 1998).

MATERIAL AND METHODS

Chemicals

1,2-Dioleoyl-3-trimethylammonium-propane (DOTAP, purity >99%, *1*; see below) and 1,2-dioleoyl-*sn*-glycero-3-phosphoethanolamine (DOPE, purity >99%, *2*; see below), were purchased from Avanti Polar Lipids (Alabaster, AL) and used without further purification.

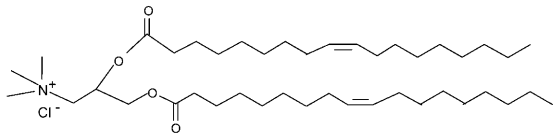

1

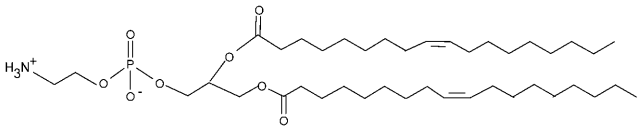

2

1,2-Dicarbadodecaborane, henceforth referred to as orthocarborane (OCB, purity 98%) was purchased from Boron Biological (Mt. Airy, NC) and used as received. Its structure, in the ball-and-stick representation, is reported in Scheme 1.

1,2-Dicarba-closododecaboran(12)-1-ylmethyl]-β-D-glucopyranoside (Glucosyl-carborane, GCOB, *3*; see below) and 1,2-dicarba-closododecaboran(12)-1-ylmethyl](β-D-galactopyranosyl)-(1$\rightarrow$4)-β-D-glucopyranoside (Lactosyl-carborane, LCOB, *4*; see below) were a gift of professor Luigi Panza, University of Piemonte Orientale, Italy, and were synthesized as described elsewhere (Giovenzana et al., 1999).

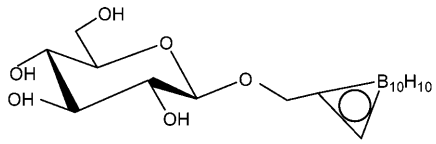

3

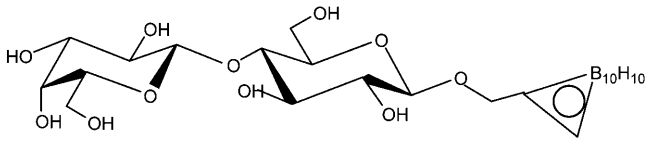

4

The three boronated compounds used in this work had the same carborane unit and differed only for the presence of one (or two) sugar ring(s).

Deuterated water (99.95% purity) was purchased from Isotech (Isotech North America, Williston, VT).

Liposome preparation

Liposomes made up by DOTAP and DOPE, in the weight ratio 1:1, were prepared as follows. Multilamellar dispersions were obtained by evaporating the solvent ($CHCl_3$) from a 10^{-2} mol/dm^3 stock solution and adding the appropriate amount of D_2O. Monolamellar, monodisperse liposomes were obtained by the well-established procedure (MacDonald et al., 1991) of freeze-and-thaw (eight cycles of plunging in liquid nitrogen, then in a water bath at 50°C, and finally vortexing) followed by extrusion through polycarbonate membranes of 100-nm pore diameter (Liposofast apparatus; Avestin, Ottawa, Ontario, CN) with 27 passages. To prepare the composite systems, the appropriate amount of carborane, dissolved either in $CHCl_3$ (OCB) or methanol (GCOB and LCOB), was added to the lipid chloroform

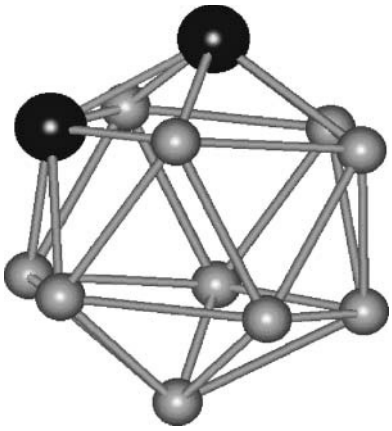

SCHEME 1 Structure of the carborane cage ($C_2B_{10}H_{12}$) in the ball-and-stick representation. Hydrogen atoms have been omitted for clarity.

solution before solvent evaporation. This allowed the best mixing among different molecules to obtain co-vesicled samples, i.e., samples in which lipids and carboranes were extruded together. In the case of LCOB, whose water solubility is considerably higher than the two other carboranes used in this work, addition after liposome formation was also possible. Non-co-vesicled samples were then obtained by depositing the LCOB/methanol solution in the bottom of a vial, followed by complete solvent evaporation and, finally, by the addition of the preformed liposome solution.

All samples contained a total lipid concentration of 4.2 10^{-2} mol/dm^3 and were prepared in D_2O. Although for x-ray experiment D_2O is not necessary, the same systems were used for both SANS and SAXS. This was done to avoid any isotopic effect from the solvent, which would imply different hydrogen bond strength and, therefore, different sugar hydration (Zhang et al., 1999; Söderman and Joanson, 2000). Carborane content was invariably expressed as molar fraction with respect to the lipid+carborane ensemble.

Density measurements

Density values were used to obtain molecular volumes. GCOB and LCOB molecular volumes were not available from the literature and, although several theoretical studies (Hermansson et al., 1999; Türker, 2003; Martin et al., 1996) on crystallographic data (The Cambridge Structural Database; http://www.ccdc.cam.ac.uk/prods/csd/csd.html) could provide structural information on the carborane cage (i.e., OCB), it has to be noted that the volumes reported are extremely scattered, ranging from 70 to 80 Å^3 per molecule (Valliant et al., 2002) to 503 Å^3 per molecule (Türker, 2003). The reasons for this mismatch are not yet clear.

In the present work, the density of the carboranes was measured starting from diluted solutions in acetone (OCB, GCOB), *n*-hexane (OCB), or water (LCOB) with an Anton Paar (DMA 5000; Anton Paar, Graz, Austria) densimeter. This apparatus determines the resonant frequency in the oscillation of borosilicate U-tubes filled with the working solution, and thereby calculates the density of the liquid. Typically, four solutions at different concentration were used for each product, and the comparison with the pure solvent allowed us to extract the following solute density: OCB, $d = 0.94 \pm 0.05$ Kg/dm^3; GCOB, $d = 1.92 \pm 0.05$ Kg/dm^3; and LCOB, $d = 1.99 \pm 0.05$ Kg/dm^3.

Molecular volume of carboranes from theoretical calculations

Standard ab initio and density functional calculations were performed on OCB, GCOB, and LCOB isolated molecules by using the Gaussian 98 package (Frisch et al., 1998), implemented on a SGI ORIGIN 3000 workstation. Geometry optimization was obtained with the RHF and B3-LYP methods, and with the 6-31G** basis set. The single bond distances, obtained for the carbon and boron atoms of the cage, were in good agreement with the results of similar calculations carried out by Hermansson et al. (1999).

Excluded volumes were calculated on the optimized structures by the Connolly method (Connolly, 1994), using a molecular probe of 1.4 Å diameter (Chem3D 8.0 software, CambridgeSoft, Chicago, IL). The following volumes were thus obtained: OCB, 148 Å^3/molecule; GCOB, 295 Å^3/molecule; and LCOB, 423 Å^3/molecule, which are to be compared with molecular volumes calculated from the density values of OCB, 255 Å^3/molecule; GCOB, 291 Å^3/molecule; and LCOB, 415 Å^3/molecule.

The agreement is very good for GCOB and LCOB, whereas in the case of the simple carborane cage, the two methods gave different results.

SAXS measurements

Small angle x-ray scattering experiments were performed on a homemade setup (Zemb et al., 2003), using a rotating anode with a copper target as the radiation source. The design of the camera is such that it allows to measure signals as weak as a 10th of that of pure water. Samples were put into 1-mm-thick cells with Nalophan windows (Nalophan BF, Kalle, Wiesbaden, Germany), that gives very weak parasitic scattering. The geometry of this instrument is fixed, and the available q-range is 0.02–0.45 Å^{-1}. Thanks to the highly monochromatic x-ray beam obtained by the optics before the sample, data reduction to the absolute scale can be performed in a simple way by using a semitransparent beam-stopper of calibrated attenuation. Thus, all SAXS spectra were acquired at the absolute scale. The detector used was a two-dimensional gas detector (Gabriel, 1977). Due to a quasipunctual collimation and to the above-mentioned high monochromaticity of the incident beam, the scattering vector resolution Δq was 0.004 Å^{-1}, which did not require any desmearing procedure.

Each spectrum was accumulated during 4 h, to reach a satisfactory signal/noise ratio.

SANS measurements

Small angle neutron scattering experiments were performed on the research nuclear reactor ORPHEE, using the PAXY instrument of the Laboratoire Léon Brillouin (Saclay, France). To cover a wide q-range, three different configurations were used. To reach low q-values, the selected neutron wavelength λ was 12 Å and the sample-detector distance D was set to 5 m. The intermediate q-value configuration was $\lambda = 4$ Å and $D = 5$ m, whereas the large q-range was obtained by using $\lambda = 4$ Å and $D = 1$ m. The overall q-range obtained for the three configurations was 0.0047–0.55 Å^{-1}. Neutron collimation before the sample was defined by three different diaphragms and tuned when changing the sample-detector distance. The detector used was a two-dimensional BF_3-gas detector. Finally, note that the size of the detector pixel was constant and that all spectral points were taken into account to build the apparatus function $R(q,\Delta q)$, which was used in the fitting procedure, as described below. Sample transmission was measured for all three configurations used in this work, and this allowed an original, in situ determination of the boron content, due to the high neutron absorption cross section of ^{10}B, as will be explained later in the text.

The flux of the direct beam was measured using a calibrated plexisheet as the attenuator for data reduction to the absolute scale. The absolute signal of H_2O was found at the correct level in the high q-range. The lower q-range was calibrated by overlapping the signal with the spectrum obtained in the intermediate q-range.

As described above, all liposome solutions were prepared in deuterated water, but the starting products contained ^{1}H atoms ($\sim$2% of the total hydrogen), and their exact amount had to be determined in order to subtract the correct value of incoherent scattering from the raw data. This calculation was performed by comparing the experimental spectra with the signal scattered by mixtures of H_2O-D_2O in the weight ratio 0:100 to 3:97. As shown in Lindner and Zemb (2002), the flat background arising from incoherent scattering is able to appreciably affect the signal only in the intermediate and large q-range, where the coherent signal tends to be 0.

DATA TREATMENT AND ANALYSIS

Method for SAXS fitting at the absolute scale

Liposomes are composite objects, and x rays are sensitive to their differences in chemical composition. In a general way, monolamellar liposomes can be described as hollow particles, which are represented by four concentric shells with the radii R_i; $R_i + t_h$; $R_i + t_h + t_c$; and R_o. Scheme 2 summarizes the geometrical features of this system and reports the physical and structural parameters used in our data treatment. The electronic density profile, which is relevant for x-ray scattering, is sketched on the left side, whereas

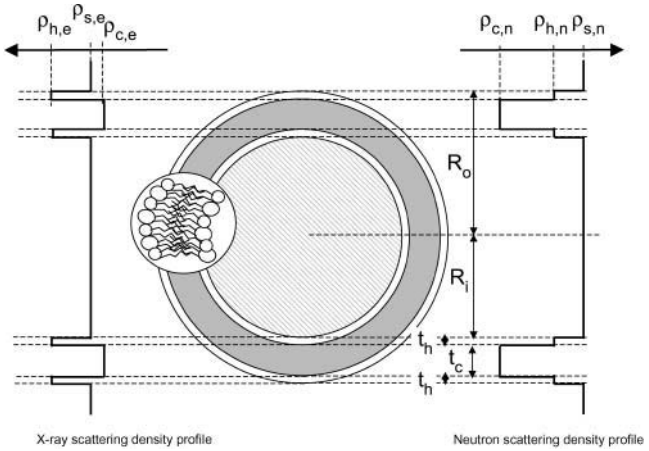

SCHEME 2 Sketch of a liposome global structure and length scattering density profile for x-ray scattering (*left side*) and neutron scattering (*right side*).

the scattering length densities for neutrons are reported on the right side.

In the case of x rays, the scattering length density of the bilayer hydrophilic part ($\rho_{h,e}$) is higher than the scattering length density of water ($\rho_{s,e}$) and, in turn, the latter is above the value of the hydrophobic core ($\rho_{c,e}$). Due to this subtle balance, the intensity scattered at low q is quite weak and a low background setup, such as ours, is required. The q-range accessible on this SAXS apparatus (0.02–0.45 A^{-1}) allowed us to probe the inner structure of the bilayers, but the outer size and shape of liposomes were not accessible. Thus, the scattered intensity in the q-range of interest can be written as (Cantù et al., 1998)

$$I(q) = \frac{4\pi}{q^4}\Sigma\left[(\rho_{c,e}-\rho_{h,e})\sin\left(q\frac{t_c}{2}\right) + (\rho_{h,e}-\rho_{s,e})\sin\left(q\frac{2t_h+t_c}{2}\right)\right]^2, \quad (2)$$

where t_c is the thickness of the hydrophobic layer and t_h is the thickness of the hydrophilic polar head layer. Σ is the surface extension of the bilayers per unit volume of solution (note that with the chosen definitions, each side of the bilayer contributes separately to Σ).

The amount of bilayer surface Σ was calculated knowing the weight fraction of lipids and carboranes in solution. The density of mixed bilayers was calculated from the values obtained by density measurements, and taking 0.92 Kg/dm^3 for the lipid mixture. Data were fitted at the absolute scale by using Eq. 2, averaged over polydispersity in the thicknesses t_c. A Gaussian distribution (having half-height width δt_c) was used. Thus, fitting to the experimental data was done by varying the five parameters of t_c; t_h; δt_c; $\rho_{c,e}$; and $\rho_{h,e}$. The step in $t_{c,h}$ was 0.4 Å, whereas the step in δt_c was 0.2 Å.

Agreement between the model and the experimental points was estimated by a χ^2 test:

$$\chi^2 = \sum_{N-2}\left[\left(\log I_{model}(q) - \log I_{exp}(q)\right)/E(q)\right]^2/(N-2), \quad (3)$$

where N is the number of points in the experimental curve and $E(q)$ is the statistical error of the intensity for a scattering q. The estimation of χ^2 on the logarithm of the intensity considerably improved the data fitting at high q where the intensity was low.

The best-fit values are reported in Table 1.

The structural parameters that allow a correct fit of the x-ray spectra must be the same as those used in the simulation of SANS spectra at large q-values, and the scattering length densities for both techniques ($\rho_{h,e}$, $\rho_{c,e}$ and $\rho_{h,n}$, $\rho_{c,n}$ for x rays and neutrons, respectively) have to be calculated with the same molecular volume for each bilayer part and with the same hydration rate for the hydrophilic portion.

Finally, note that the fitting procedure in the case of neutron scattering curves mostly involved the thickness of the hydrophobic layer t_c, since the scattering length density of the hydrated polar head region was very close to the solvent value. However, SANS fittings still allowed us to determine both the form and shape of liposomes, as discussed in the next section.

Method for SANS fitting at the absolute scale

For spherically symmetric vesicles, the scattering cross section per unit volume V can be written as

$$I(q)[cm^{-1}] = \frac{n}{V}P(q)S(q), \quad (4)$$

where n is the total number of particles in the sample, V the sample volume, $P(q)$ the particle form factor, and $S(q)$ the structure factor. The prefactor n/V can be expressed as to $\Phi/V_{bilayer}$, where Φ is the volume fraction of lipids in the sample and $V_{bilayer}$ the total bilayer volume of a vesicle.

Scattering from our dilute vesicle solutions did not exhibit any correlation peak; therefore, the structure factor $S(q)$ could be assumed to be *1* in the whole q-range investigated.

The form factor of three concentric shells with radii R_i and length scattering densities ρ_i, $i = 1,3$ ($i = 1$ being the external layer) is given by Pedersen (1997) as

$$P(q) = \left[\sum_{i=1}^{4} V_i(\rho_i - \rho_{i+1})F(q,R_i)\right]^2, \quad (5)$$

and can be developed as

$$P(q) = \left[V_o(\rho_{h,n} - \rho_{s,n})F(R_o) + V_{Ri+th+tc}(\rho_{c,n} - \rho_{h,n}) \times F(R_i + t_h + t_c) + V_{Ri+th}(\rho_{h,n} - \rho_{c,n}) \times F(R_i + t_h) + V_i(\rho_{s,n} - \rho_{h,n})F(R_i)\right]^2, \quad (6)$$

where

TABLE 1 Physical parameters for plain and carborane-loaded liposomes, used in the fitting of SAXS and SANS spectra

X-ray Neutrons	Density	$\rho_{c,e}$ (cm^{-2})	$\rho_{h,e}$ (cm^{-2})	$\rho_{c,n}$ (cm^{-2})	$\rho_{h,n}$ (cm^{-2})	t_c (Å) δt_c	t_h(Å)	e (Å) X e (Å) n	R_0 (Å)	σ*
DOTAP/DOPE	0.92	$7.6\ 10^{10}$	$1.32\ 10^{11}$	$-2.08\ 10^{9}$	$3.5\ 10^{10}$	28.0	5.4	38.8	445	0.13
Pure liposomes						0.9				
DOTAP/DOPE	0.935	$7.8\ 10^{10}$	$1.28\ 10^{11}$	$-1.29\ 10^{9}$	$3.5\ 10^{10}$	28.0	5.4	38.8	353	0.14
+ $X_{OCB} = 0.25$						1.0				
DOTAP/DOPE	1.17	$7.7\ 10^{10}$	$1.38\ 10^{11}$	$-1.18\ 10^{9}$	$3.48\ 10^{10}$	26.0	5.4	36.8	432	0.13
+ $X_{GCOB} = 0.25$						1.0				
DOTAP/DOPE	1.27	$7.7\ 10^{10}$	$1.38\ 10^{11}$	$-6.82\ 10^{9}$	$3.75\ 10^{10}$	27.2	5.6	38.4	513	0.12
+ $X_{GCOB} = 0.35$						1.2				
DOTAP/DOPE	1.42	$7.6\ 10^{10}$	$1.38\ 10^{11}$	$2.61\ 10^{8}$	$4.12\ 10^{10}$	26.0	6.0	38.0	503	0.16
+ $X_{GCOB} = 0.50$						0.5				
DOTAP/DOPE	1.08	$7.8\ 10^{10}$	$1.25\ 10^{11}$	$-1.61\ 10^{9}$	$4.45\ 10^{10}$	28.0	8.0	44.0	402	0.2
+ $X_{LCOB} = 0.15$ cov.						1				
DOTAP/DOPE	1.19	$7.8\ 10^{10}$	$1.27\ 10^{11}$	$-1.19\ 10^{9}$	$4.75\ 10^{10}$	28.0	7.5	43	385	0.17
+ $X_{LCOB} = 0.25$ cov.						1.6				
DOTAP/DOPE	1.29	$7.8\ 10^{10}$	$1.27\ 10^{11}$	$-6.89\ 10^{9}$	$5.09\ 10^{10}$	26.0	9.0	44	420	0.24
+ $X_{LCOB} = 0.35$ cov.						1.2				
DOTAP/DOPE	1.45	$7.6\ 10^{10}$	$1.28\ 10^{11}$	$2.61\ 10^{9}$	$5.46\ 10^{10}$	24.0	10.0	44	459	0.18
+ $X_{LCOB} = 0.50$ cov.						2.0				
DOTAP/DOPE	1.08	$7.6\ 10^{10}$	$1.27\ 10^{11}$	$-2.01\ 10^{9}$	$2.02\ 10^{10}$	27.0	8.0	43	354	0.14
+ $X_{LCOB} = 0.15$ n.c.						1		37.8		
DOTAP/DOPE	1.19	$7.5\ 10^{10}$	$1.29\ 10^{11}$	$-1.96\ 10^{9}$	$1.81\ 10^{10}$	26.6	7.5	41.6	360	0.14
+ $X_{LCOB} = 0.25$ n.c.						1.4		37.6		
DOTAP/DOPE	1.29	$8.0\ 10^{10}$	$1.23\ 10^{11}$	$-1.88\ 10^{9}$	$1.57\ 10^{10}$	22.0	10.0	42.0	346	0.14
+ $X_{LCOB} = 0.35$ n.c.						1.6		37.6		
DOTAP/DOPE	1.45	$7.80\ 10^{10}$	$1.23\ 10^{11}$	$-1.73\ 10^{9}$	$1.23\ 10^{10}$	24.0	12.0	48.0	392	0.16*
+ $X_{LCOB} = 0.5$ n.c.						1.6		39.8		

The meaning of all symbols is explained in the text. In particular: cov = covesicled; n.c. = not covesicled.
*The oscillations are low, and impossible to fit correctly with a spherical model.

$$F(r_i) = 3\left[\frac{\sin(qr_i) - qr_i\cos(qr_i)}{(qr_i)^3}\right] \quad (7)$$

is the standard form factor of a homogeneous sphere.

The general fitting method was as follows: first, SAXS data were simulated using Eq. 2, and this gave the best-fittings values reported in Table 1. Second, the amount of water hydrating the polar heads was deduced, following the procedure described in Results and Discussion, below. Third, from the partial molar volume and deduced composition of each part of the bilayer (including the number of water molecules bound to each polar head), the neutron scattering length densities of both the heads ($\rho_{h,n}$) and the hydrophobic core ($\rho_{c,n}$) were calculated.

Note that for the liposomes studied in this work, a one-shell model gave fits of equivalent quality to those obtained with the proposed three-shell model. In fact, the polar head thickness was small compared to the thickness of the hydrophobic core and differences between the two models showed up only at large q (>0.2 Å^{-1}), that is, in a domain where it was difficult to extract the scattered signal from the incoherent background. Nevertheless, we chose to use the three-shell model to be consistent with the x-ray data analysis.

The SANS experimental intensity suffers from a smearing of Eq. 4 by the size distribution of scattering objects and by the instrumental resolution. The form and relative weight of these two contributions are detailed elsewhere (Grillo, 2000) and the final equation we chose for our modeling procedure can be written as

$$I_{model}(q) = \int_0^\infty R(q, \Delta q, q') \times \int_0^\infty K_c G(R_i, \sigma*, r') F^2(r', q') dr' dq', \quad (8)$$

where the instrumental resolution $R(q,\Delta q,q')$ is represented as a Gaussian function and the polydispersity $G(R_i,\sigma*,r')$ is characterized by a log-normal distribution with a full width at half-maximum of $2R_0\sigma*$. The same χ^2 test was used to estimate the quality of the fitting, as explained in Method for SAXS Fitting at the Absolute Scale, above.

The differences in instrumental resolution between the configurations used to cover the broad q-range were constrained to separately fit the small angles ($4.0\ 10^{-3} < q$ (Å^{-1}) <0.09) and the large angles (q (Å^{-1}) >0.09) data. The range of small q allowed us to extract the radius of liposomes and their polydispersity in size. The thicknesses of the different layers that constitute the liposome membrane were obtained from the fitting of SAXS data, as mentioned before. The only unknown parameters were R_i (the inner radius), and σ. The program varied R_i by 0.1 Å

steps and σ^* by 0.05 steps between given minimal and maximal approximate values. The value χ^2 was evaluated for each iteration and the parameters giving the smallest χ^2 were retained. We estimated the relative error on the radius R_i as 5%.

RESULTS AND DISCUSSION

Boron content determination from ^{10}B neutron absorption cross section

The exact boron content in DOTAP/DOPE liposomes loaded with carboranes was not known from the preparation procedure, because several experimental steps are required to obtain the final samples, and the carboranes used in this work have a solubility in water that is less than the theoretical value of most samples. Standard analytical techniques, such as ICP-MS, failed to give good accuracy and reproducibility, probably due to the complex nature of the matrix in which boron is embedded or to the high boron concentration in these systems.

Carborane insertion into lipid bilayers is expected to take place easily, because of the well-known lipophilic character of the carborane cage (Escher et al., 1980; Pliška et al., 1981). Indeed, several authors have suggested using the $-C_2B_{10}H_{11}$ unit to increase the penetration of drugs inside the cell membrane, without any reference to boron-related therapies (Yamamoto and Endo, 2001; Endo et al., 2001). Moreover, the choice of using dioleoyl hydrocarbon chains allowed us to work with fluid bilayers, since for this kind of lipid the $L_\alpha \rightarrow L_\beta$ transition is known to occur below 0°C (Cevc, 1993). In principle, this should favor local deformations to accommodate host molecules, even though the latter have a completely different shape, as in the case of the icosahedral carborane cage.

In this work, boron concentration in carborane-containing liposomes was calculated from neutron transmission values, taking into account that, in the thermal range of energy ($E \leq$ 0.3 eV), the absorption of neutrons by ^{10}B can be totally attributed to the fission reaction (Eq. 1). This assumption does not bring any relevant limitation to analytical methods, and it has been adopted for boron determination in chromatography (Kvítek et al., 1975), where high accuracy is required. Solid-state neutron detectors based on carboranes have already been proposed (Robertson et al., 2002), and have been shown to work with high sensitivity, even when the starting carboranes are not isotopically enriched with ^{10}B.

Nevertheless, up to now, the transmission method for quantitative determination of boron (Szegedi et al., 1990) has rarely been used.

Transmission can be written as

$$T = \frac{N}{N_0} = e^{-n_a \sigma_a d}, \quad (9)$$

where N_0 and N are the incident and transmitted neutron flux, respectively; n_a is the number of absorbing nuclei per volume unit; d is the sample thickness; and σ_a is the neutron absorption cross section.

Transmission was measured for all the samples in each experimental configuration and normalized with respect to pure liposomes, dividing by their transmission value in the same experimental conditions. This could be done because lipid content was kept constant in all the preparations. The obtained values thus contained only the absorption due to glycosyl carboranes, which are made of C, H, O, and B atoms. Neutron absorption cross sections for all the isotopes of these elements are at least 3–4 orders-of-magnitude lower than the ^{10}B value (see tables reported in *Neutron News*, 1992, 3:29–37); therefore, they were neglected. This approximation, though fully justified a priori by tabulated cross-sections and isotopic compositions of the involved atomic species, was also validated a posteriori by the results obtained in our calculation, as shown in the following.

In the thermal range, σ_a is inversely proportional to the neutron speed—that is, to the square-root of the energy ($E = 1/2\ mv^2$), and the proportionality constant for ^{10}B is 611 (Hughes and Schwartz, 1958). The neutron speed v was calculated from the associated wavelength ($v = \hbar/m\lambda$, where m is the neutron mass and $\hbar$ the Plank's constant), thus obtaining $v = 985.1$ m/s ($\sigma_a = 8.586\ 10^{-12}$ m^2) for $\lambda = 4.03$ Å, and $v = 330.8$ m/s ($\sigma_a = 2.557\ 10^{-12}$ m^2) for $\lambda = 12.0$ Å.

The cell thickness d was 2 mm. Assuming that all concentrations in the final samples were the same as those in the starting solution— that is, before liposome extrusion—all quantities in Eq. 9 were known and the absorption coefficient $\mu = n_a\ \sigma_a$ could be calculated.

Fig. 1 *a* shows the experimental absorption coefficients of GCOB-loaded liposomes and the corresponding theoretical lines as a function of carborane content. The higher error reported for $\lambda = 12.0$ Å was a consequence of the lower flux obtainable at low neutron energy in the PAXY beam line.

As explained above, the fitting trend was calculated with no adjustable parameters, and this showed that practically all GCOB used in the preparation was incorporated into liposomes. A similar behavior was found for LCOB, either if co-vesicled with lipids (as in the case of GCOB), or added to preformed liposomes.

However, in the case of the simple icosahedral cage (OCB), only a partial incorporation could be obtained, as shown in Fig. 1 *b*. This meant that the presence of the polar head played an important role in lipid-carborane mixing, and that dipole-dipole interactions added a favorable contribution. Indeed, homogeneous mixing of a sugar-based amphiphile with a tetraalkylammonium double-chain surfactant has been reported in the literature up to a high glycolipid content (molar fraction $\leq$ 0.75) (Ricoul et al., 1998).

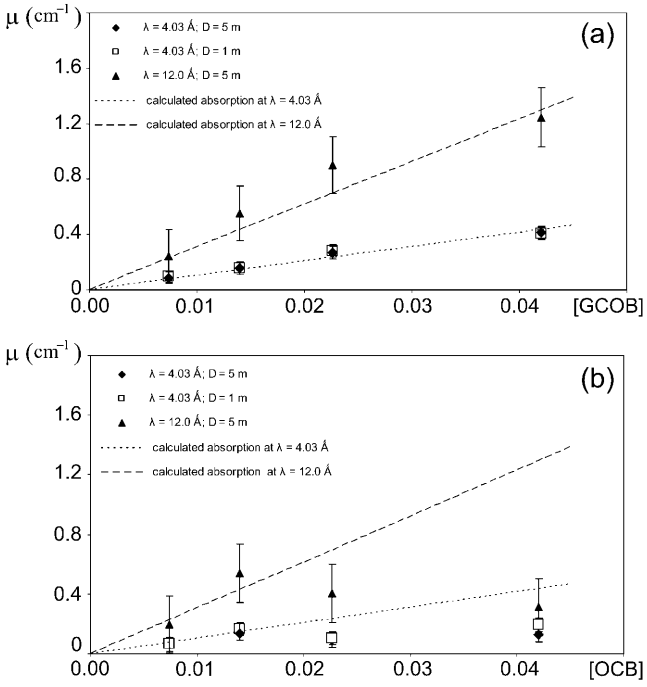

FIGURE 1 Neutron absorption coefficient versus theoretical (i.e., starting) content of glucosyl-carborane (*a*) and orthocarborane (*b*) in loaded liposomes.

Structure of the liposomes

The five types of liposomes that were examined are presented in a sequence, going from pure liposomes to the more complex systems.

Liposomes without carborane addition

The SAXS and SANS scattering diagrams of plain DOTAP/DOPE liposomes are shown in Figs. 2 and 3, respectively, together with the corresponding best fits, which were obtained using the physical characteristics listed in Table 1.

Two sets of important conclusions can be drawn. First, these vesicles were really unilamellar since both the SAXS and SANS fits, based on this assumption, worked at the absolute scale and used the same parameters. From the SAXS spectrum the total thickness was found to be 38.7 Å, in very good agreement with the value reported by Radler and co-workers (39 ± 0.5 Å) for the same bilayer in a similar system (Radler et al., 1997). Moreover, the oscillations in the SAXS diagrams were marked, showing that the bilayer thickness was well defined. This could be quantified by the small width of the distribution thicknesses extracted from the fitting procedure, which is <7% for the total bilayer. Secondly, from the SANS fitting we found that DOTAP/DOPE liposomes were actually spherical objects, and that their size could be determined from the oscillation at low q. The obtained value for the outer radius was 445 Å and the width of its log-normal distribution was fairly low ($\sigma = 0.14$).

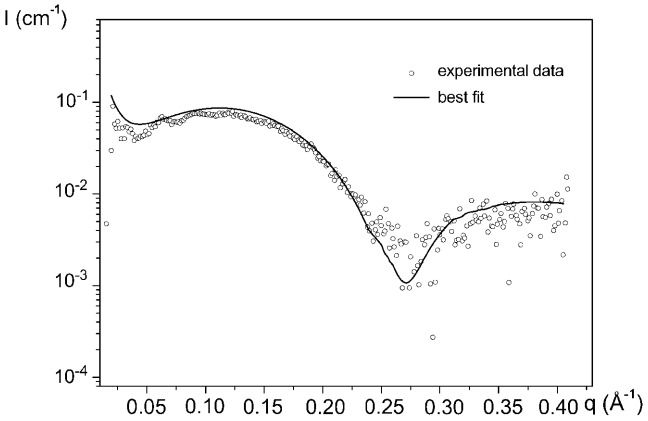

FIGURE 2 SAXS profile for DOTAP/DOPE pure liposome. Total lipid concentration: 4.2 10^{-1} mol/dm^3. The best-fit parameters are reported in Table 1.

More details on the structure of liposomes could be gained by performing a deeper analysis of SAXS data. In fact, from the mass density d_m (kg/m^3) of the bilayer, a total molecular volume v_m (Å^3) of the DOPE/DOTAP mixed surfactant could be calculated as

$$v_m = 10^{24}\frac{M_w}{d_m N_A}, \tag{10}$$

where M_w is the averaged molar mass of DOTAP and DOPE. This volume was split into a hydrophobic part $v_{m,c}$ and a hydrophilic part $v_{m,h}$. From the scattering length density of each bilayer part, the corresponding volume was calculated. For the hydrophobic core, which does not contain water, the calculation is trivial,

$$\rho_{c,e} = \frac{Z_c L_T}{v_{m,c}}, \tag{11}$$

where Z_c is the number of electrons in the hydrophobic chains ($Z_c = 270$) and L_T the electron scattering length

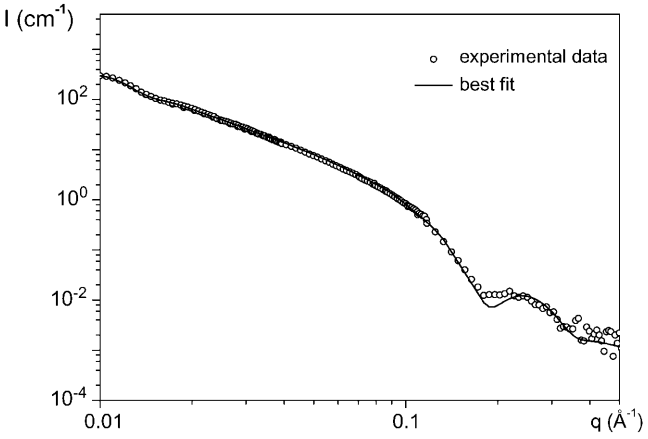

FIGURE 3 SANS profile for DOTAP/DOPE pure liposome. Total lipid concentration: 4.2 10^{-1} mol/dm^3. The best-fit parameters are reported in Table 1.

($2.82\ 10^{-13}$ cm). For the hydrophilic heads, which are hydrated by n water molecules each, the scattering length density can be written as

$$\rho_{h,e} = \frac{(Z_h + n\ Z_{H_2O})L_T}{v_{m,h} + n * v_{H_2O}}, \quad (12)$$

with Z_h being the average electron number of the polar head (126), v_{H2O} the molecular volume of water (30 Å^3), and Z_{H20} its number of electrons (i.e., 10). The ratio between the two-part thicknesses is linked to their respective volume by

$$\frac{2\,t_h}{t_c} = \frac{v_{m,h} + n\ v_{H_2O}}{v_{m,c}}. \quad (13)$$

Using Eqs. 10 and 11, we slightly adjusted d_m to get the correct scattering length density of the hydrophobic core. Then, from Eq. 12, the number of water molecules n per hydrophilic head was obtained, by matching the calculated value and measured value of the hydrophilic scattering length density $\rho_{h,e}$. Finally, the resulting hydrophilic thickness was deduced from Eq. 13. The best agreement was obtained using $d_m = 0.965$ kg/m^3. The results of this calculation are reported in Table 2.

Addition of orthocarborane to DOTAP/DOPE liposomes

As outlined in the previous section, neutron absorption measurements showed that the maximum loading of the icosahedral OCB into DOTAP/DOPE vesicles was obtained for $X = 0.25$. The four scattering diagrams, corresponding to OCB molar fraction from $X = 0.15$ to $X = 0.5$, are reported in Fig. 4. In the intermediate q-range, the scattering by liposome decreases as q^{-2}, since, at an intermediate scale, a liposome is like a plane of finite thickness. Therefore, the $q^2I(q)$-versus-q representation was used to enlighten possible shape transformations, which are mainly reflected in the low q-region of the spectra. It was observed that liposomes with varying OCB-loading ratio were actually different from one another. Moreover, due to the insertion of the carborane molecules, the size of liposomes was slightly decreased with respect to pure liposomes, as shown in Table 1.

Nevertheless, the most important result was the loss of spherical shape for carborane addition higher than $X = 0.25$. In fact, the two oscillations observed at low q could not be correctly fitted with any reasonable polydispersity. The conclusion was therefore twofold: 1), orthocarborane molecules could not be inserted into the lipid bilayer above a given threshold; and 2), they modified the shape of liposomes at tentatively high loading ratios. This effect was not trivial to model but, in any case, bilayer stress and deformation, with consequent loss of the spherical shape, cannot be considered as a favorable property for the penetration of liposomes into tumor cells. Indeed, the loss of spherical shape is often accompanied by an increase in size.

TABLE 2 Partial molecular volumes, number of hydrating molecules and polar head thickness in plain and carborane-loaded liposomes

	$v_{m,c}$ Initial (Å^3) δ $v_{in,c}$	$v_{m,h}$ Initial (Å^3) δ $v_{in,h}$	No. of D_2O/ polar heads	Hydrophilic thickness (Å) from SAXS fits	Hydrophilic thickness (Å) calculated*
Pure liposome	1003	261	3.2	5.4	5.0
	0	0			
DOTAP/DOPE	1003	261	2.0	5.4	4.5
+ $X_{OCB} = 0.25$	185	0			
DOTAP/DOPE	1003	261	2.5	5.4	4.7
+ $X_{GCOB} = 0.25$	250	106			
DOTAP/DOPE	1003	261	3.3	5.6	5.6
+ $X_{GCOB} = 0.35$	265	106			
DOTAP/DOPE	1003	261	4.7	6	6.5
+ $X_{GCOB} = 0.50$	300	106			
DOTAP/DOPE	1003	261	6.8	8	7.4
+ $X_{LCOB} = 0.15$ cov.	160	231			
DOTAP/DOPE	1003	261	7.8	7.5	8.4
+ $X_{LCOB} = 0.25$ cov.	220	231			
DOTAP/DOPE	1003	261	9.7	9	9.5
+ $X_{LCOB} = 0.35$ cov.	245	231			
DOTAP/DOPE	1003	261	12	10	11
+ $X_{LCOB} = 0.50$ cov.	300	231			
DOTAP/DOPE	1003	261	5.9	8	6.5
+ $X_{LCOB} = 0.15$ n.c.	295	231			
DOTAP/DOPE	1003	261	6.9	7.5	7.4
+ $X_{LCOB} = 0.25$ n.c.	295	231			
DOTAP/DOPE	1003	261	12.2	10	9.4
+ $X_{LCOB} = 0.35$ n.c.	195	231			
DOTAP/DOPE	1003	261	15.4	12	13.4
+ $X_{LCOB} = 0.50$ n.c.	270	231			

*From Eq. 12 for plain liposomes, and from Eq. 15 for carborane-loaded liposomes.

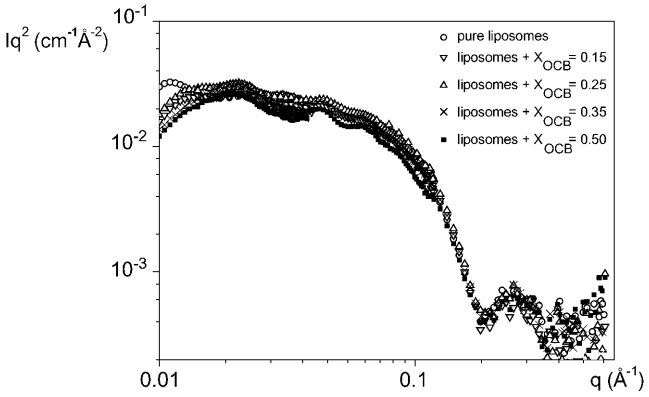

FIGURE 4 SANS spectra of plain and OCB-loaded liposomes. Total lipid concentration was 4.2 10^{-1} mol/dm^3 for all samples. The $q^2I(q)$ versus q-representation is able to evidence the different behavior of the curves in the low q-region.

On the other hand, the SAXS diagrams corresponding to the four different OCB/liposomes systems at different loading ratios were very close to one another, as shown in Fig. 5, where they are plotted together with the pure liposome spectrum.

From the absence of effects on the SAXS scattering curves it can be concluded that any influence on the bilayer structure, induced by the OCB presence, was hardly detectable. This allowed us to establish that the molecular volume of the orthocarborane cage is such that it did not modify the electronic density $\rho_{c,e}$ of the bilayer hydrophobic region to an appreciable extent. In fact, when the carborane cage bearing the $Z_{OCB} = 74$ electron is inserted in the oleoylic part, an additional volume $\delta v_{in,c}$ is to be considered to obtain the new scattering length density of

$$\rho_{c,e} = \left(\frac{((1-X)\,Z_c + X\,Z_{OCB})L_T}{(1-X)\,v_{m,c} + X\;\delta v_{in,c}} \right)^2. \qquad (14)$$

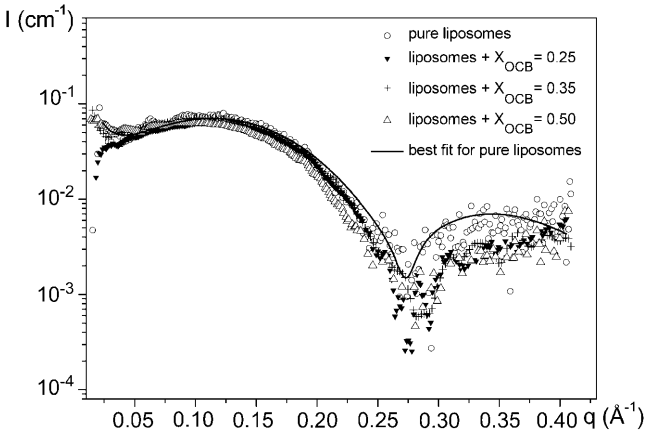

FIGURE 5 SAXS profiles for plain and carborane-loaded liposomes. The fitting of the pure liposome curve is also shown for comparison. Lipid content was 4.2 10^{-1} mol/dm^3 for all samples.

Considering the $X = 0.25$ case, the value $\rho_{c,e} = 7.80\ 10^{10}$ cm^{-2} leads to an insertion volume of 185 A^3 per molecule. This is an intermediate value between the volume obtained from ab initio calculations and the volume deduced from density measurements. As the OCB molecule is inserted in the lipophilic core, the volume it occupies inside the bilayer can be minimized by a rearrangement of the hydrocarbon chains around it, which are in a fluid state. There is no constraint on the location of the OCB molecule within the hydrophobic core. This no longer holds for the two other cases (GCOB and LCOB). Accordingly, the insertion volume obtained from the simulation of SAXS spectra (volume of the cage insertion) may represent a minimum value.

Addition of glucosyl carborane to DOTAP/DOPE liposomes

The SAXS scattering diagrams of liposomes containing glucosyl carborane are reported in Fig. 6, together with the best-fits obtained using the parameters listed in Table 1.

The SANS scattering curves of this series are not shown because they contain the same kind of information as in Fig. 6. The corresponding fits were all done with the parameters listed in Table 1.

The fitting procedure was guided by the following a priori: neutron absorption measurements have shown that all the GCOB molecules contained in the initial mixture were also present in the liposome dispersion after extrusion. Considering that GCOB solubility in water is very low ($<2.0\ 10^{-4}$ mol/l) and that these molecules do not form micelles in water solution, it was assumed that GCOB molecules were all inserted in the bilayers. Taking the density of pure GCOB as measured from the acetone solutions ($d = 1.92 \pm 0.05$ g/cm^3), the density of each GCOB/liposome sample was calculated, and the obtained values are reported in the first column of Table 1.

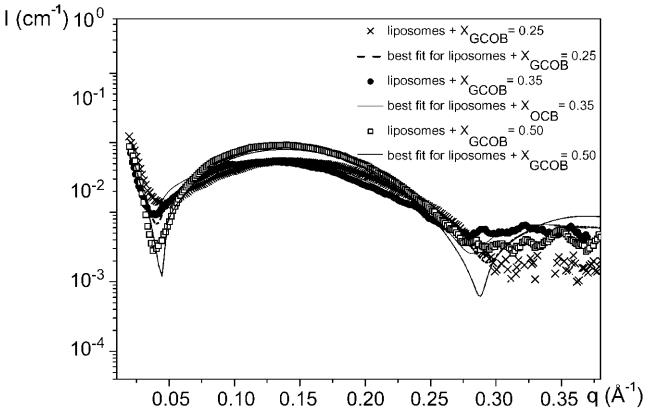

FIGURE 6 SAXS curves for liposomes loaded with different amounts of glucosyl-carborane and corresponding best fits.

From the above experimental data and scattering curve simulation, several conclusions could be drawn. First, upon GCOB addition, a small but appreciable increase in the thickness of the hydrophilic bilayer region (t_h) was observed. The SAXS scattering length was higher than in pure liposomes, but it remained substantially constant when GCOB content was increased.

Considering that neutron absorption data ensure that full uptake has occurred, we conclude that the hydrated sugar heads of GCOB were inserted in the hydrophilic region of the liposome bilayer, without extra protrusion. This was due to the small size of the glucosyl group, which is able to fit into the ~5.5 Å of the hydrophilic layer up to very high loading without a remarkable thickness variation.

Such speculation could be made more quantitative using the procedure outlined above. Again, we assumed that the carborane cage was accommodated by the oleoylic chains in the bilayer. Nevertheless, because it was anchored to an hydrophilic head, its location was forced close to the interface between the hydrophilic and hydrophobic parts. Therefore, the effective volume $\delta v_{in,c}$ required within the oleoyl chains could be different (and certainly greater) than in the pure OCB insertion. Again, Eq. 14 was used to derive the insertion volume of the carborane cage attached to a sugar head. The results are reported in Table 2. Obviously, they were slightly larger with respect to the case of OCB, when the cage is alone, but the volume depended only slightly on the rate X of insertion.

The same type of analysis could be done for the hydrophilic part where the sugar head was located. It gave $Z_G = 95$ electrons in an insertion volume of $\delta v_{in,h}$. The three types of heads are hydrated by n water molecules each, on average. This lead to a scattering length density $\rho_{h,e}$ equal to

$$\rho_{h,e} = \left(\frac{((1-X)\,Z_h + X\,Z_G + n\,Z_{H_2O})L_T}{(1-X)\,v_{m,h} + X\,\delta v_{in,h} + n\,v_{H_2O}} \right)^2. \qquad (15)$$

The agreement between the experimental value and the value calculated through Eq. 15 could be obtained using two parameters of either $\delta v_{in,h}$ or n. The insertion volume of the sugar head was considered constant and equal to its value, and deduced as follows. The density measurement showed that the GCOB molecular volume was equal to 291 Å^3. The OCB molecular volume determined from density measurement was 255 Å^3. One solution would be to take 36 Å^3 as the insertion molecular volume for the sugar head, but this value was obviously too small. Nevertheless, both theoretical simulation and SAXS fitting yielded a lower value for the insertion volume of the orthocarborane (150 Å^3 and 185 Å^3, respectively). The latter value was chosen because it came from an experimental measurement. Therefore, the insertion volume occupied by one sugar head in the hydrophilic part was taken equal to 106 Å^3.

Finally, depending on the insertion rate, the hydrophilic thicknesses are then deduced by

$$\frac{2t_h}{t_c} = \frac{v_{m,h} + \delta v_{in,h} + n\,v_{H_2O}}{v_{m,c} + \delta v_{in,c}}. \qquad (16)$$

The agreement between the calculated hydrophilic thicknesses and the actual measured one was very good. This result, as it stands, strongly supported the discussion presented here and the conclusions that have been drawn on the structure of the bilayer containing GCOB. The sugar heads were thus fully immersed in the hydrophilic layer without increasing its thickness. They also slightly increased the number of water molecules per head in the layer, but not with any marked effect.

At a larger scale, the effect on the size of the vesicle was more subtle. Indeed, for low GCOB loading, a small decrease of the outer radius was observed, whereas for a higher loading ratio the size of the vesicles slightly increased (from ~44 nm to ~50 nm, in the $X = 0.5$ system). Although a discussion of the observed vesicle sizes is not within the aims of this article, a possible explanation for the nonmonotonic evolution of the vesicle radius with carborane content is offered as follows. The final size is an equilibrium (possibly metastable) between forces favoring small vesicles (e.g., those exerted during extrusion, entropy of mixing, etc.) and the bending rigidity of the bilayer (see Helfrich's expression, in Helfrich, 1978). It has been shown that the introduction of another species with different spontaneous curvature in the bilayer (Safran, 2002; Porte and Appell, 1981) gives an additional degree of freedom for the exchange between the two monolayers. Hydration forces can also play a key role in determining the bilayer rigidity and final curvature (McIntosh, 1996). This allows the bilayer to readjust more easily to outer constraints. At high carborane content, such an effect is apparently compensated by the cage rigidifying the bilayer and by crowding of the sugar heads on the surfaces.

Finally, the most important result is that DOTAP/DOPE vesicles were not deformed or disrupted, but retained their spherical shape even at high GCOB-loading ratios (one carborane molecule to each lipid molecule). This observation allows us to state that DOTAP/DOPE liposomes containing glucosyl carborane are good candidates as boronating agents for BNCT.

Addition of lactosyl carborane to DOTAP/DOPE liposomes (co-vesicled system)

The SAXS scattering diagrams of liposomes containing co-vesicled lactosyl carborane are reported in Fig. 7. These curves were simulated with the best-fit parameters listed in Table 1.

The first minimum was better marked for LCOB-containing liposomes than for plain liposomes and, for this carborane, such an effect was related to a large increase in the thickness of the hydrophilic region. Indeed, it increased from 5.4 Å ($X_{LCOB} = 0$) to 10 Å ($X_{LCOB} = 0.5$). Nevertheless, the

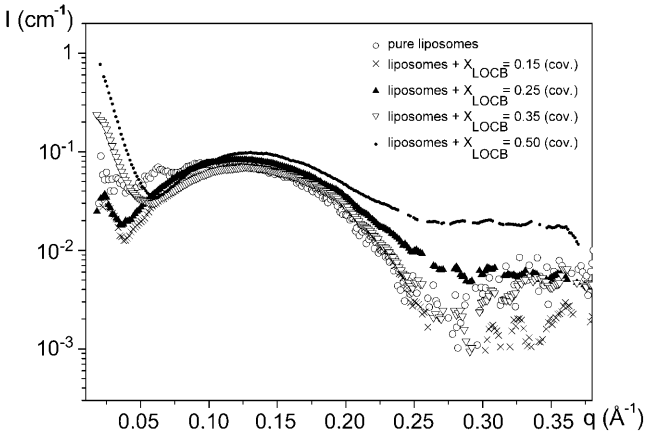

FIGURE 7 Experimental SAXS diagrams of liposomes containing LCOB, added before extrusion, at molar fractions ranging from 0 (pure liposomes) to 0.5.

scattered length density $\rho_{h,e}$ remained almost constant and even slightly decreased from 1.32 10^{11} cm^{-2} for $X_{LCOB} = 0$ to 1.28 10^{11} cm^{-2} in for $X_{LCOB} = 0.5$. As in the GCOB case, due to the cage insertion, the electronic density of the hydrophobic core slightly increased, from 7.6 10^{10} cm^{-2} to 7.8 10^{10} cm^{-2}. Furthermore, a measurable decrease of the hydrophobic thickness was observed at high loading ($t_c = 24$ Å for $X = 0.5$). Imposing a numerical agreement between the calculated and measured scattering length density of both the hydrophobic and hydrophilic parts allowed us to determine the insertion volume of the carborane cage $\delta v_{in,h}$ anchored to a double sugar head, the lactosyl head insertion volume $\delta v_{in,h}$, the number of water molecules n per head, and the thicknesses of the hydrophilic part t_h. The results are all reported in Table 2 and again, the internal consistence among different data was extremely good. It can be observed that the insertion volume of the sugar-anchored carborane cage was higher than for the pure carborane cage. Nevertheless, the volume was not higher than in the GCOB case and the only further adaptation that was imposed by the double sugar head was a lower thickness of the hydrophobic core. This could mean that the arrangement of the oleylic chain around the carborane cages was not exactly the same in the two cases (GCOB and LCOB). The double sugar could not fit the pure liposome hydrophilic layer and therefore the polar head was protruding into water beyond the moieties of the phospholipid heads. The lactosyl units also brought a large amount of water with them. This is indeed a positive feature for medical application of liposomes loaded with LCOB, because the presence of sugar on the outer surface is thought to enhance the uptake by tumor cells.

SANS spectra simulations, performed with the best-fit parameters reported in Table 1, showed that the outer radius of liposomes containing LCOB increased monotonically with increasing carborane content, although being smaller than the radius of pure liposomes, except for the highest molar fraction ($X_{LCOB} = 0.50$). This behavior was in agreement with the case of GCOB-containing liposomes, and was therefore explained by the same arguments mentioned in the previous section.

Moreover, polydispersity, which was invariably low and close to the value of pure liposomes, strongly pushed toward substantial retention of the spherical shape after lactosyl carborane insertion. No major stress and deformations took place in the host structure, which showed itself, once again, to be stable and flexible enough to accommodate large quantities of guest sugar-carborane molecules. For the highest insertion rate, the total number of boron atoms present in the liposome could be deduced by

$$N(B) = \frac{10\ 2\ S_{Lipo} t_c}{(1 - X)\, v_{m,c} + X\ \delta v_{m,c}}, \tag{17}$$

where S_{lipo} is the outer surface of the liposome. For $X = 0.5$, this gave $N(B) = 2\ 10^6$ boron atoms per liposomes.

The above calculation indicates that, in the case where this type of carrier is able to localize close to the cell nucleus, just 100–200 of them would be enough to destroy a malignant cell through neutron capture.

Addition of lactosyl carborane after liposome formation (not co-vesicled systems)

The presence of all LCOB molecules in the samples was assessed by neutron transmission experiments. The SAXS and SANS curves, of liposomes containing LCOB added after extrusion, were not exactly the same as the corresponding systems where LCOB had been added before liposome formation. An example of this situation is given in Fig. 8, where the SAXS diagrams of the two $X_{LCOB} = 0.5$ systems are reported, together with the corresponding simulations.

Structural differences between the two series of LCOB-containing liposomes were not large, as illustrated by the different best-fit parameters used to reproduce the experimental data, which are listed in Tables 1 and 2.

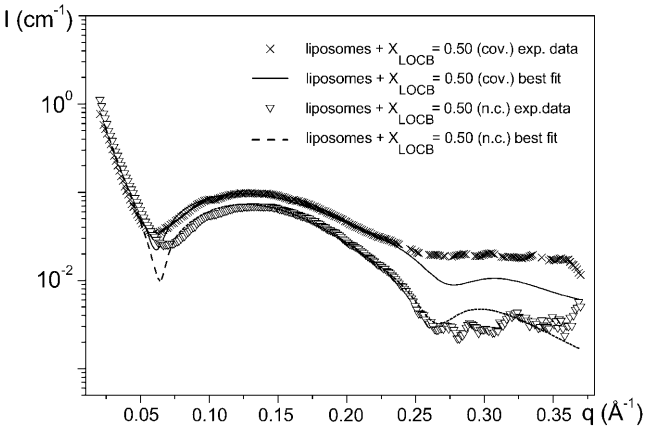

FIGURE 8 SAXS spectra, with corresponding simulations, of co-vesicled and non-co-vesicled $X_{LCOB} = 0.25$ samples.

It was clear that sugar heads were protruding beyond the heads of the phospholipids and that the orthocarborane cage was also inserted in the hydrophobic region, in the case of carborane added to preformed liposomes. Therefore the structure of the bilayer was close to that obtained with co-extrusion. Finally, the outer radius of liposomes, determined from SANS curve simulations, increased with increasing LCOB content (as happened in co-vesicled samples), but its value was invariably lower than in the case of covesicled sample.

CONCLUSIONS

In this article the insertion of different carboranes into DOTAP/DOPE liposomes was quantified by neutron absorption experiments, and the structural properties of the loaded systems were studied by combining the use of small angle neutron and x-ray scattering.

Of the three carboranes investigated, only OCB—which does not possess a polar part—showed incomplete loading, although the maximum value reached (approximately one carborane molecule to each three lipids) should not be considered a poor insertion rate.

Glucosyl carborane and lactosyl carborane were fully uptaken by DOTAP/DOPE liposomes to a high molecular fraction ($x = 0.5$; that is, one carborane molecule for each lipid). Extensive data treatment, based on the simultaneous fitting of the SAXS and SANS curves at the absolute scale, showed that the sugar moieties were included in the polar head layer of liposomes. In the case of LCOB, definite protrusion of the lactose double-ring was observed and the corresponding protrusion length was calculated.

Some differences were found in the composite structures according to different loading procedures, but in no case were the original liposomes disrupted. On the contrary, a substantial retention of their global size and shape was demonstrated.

The results obtained in this work indicate that DOTAP/DOPE liposomes, loaded with sugar-derived carboranes, can be considered potent boron carriers for BNCT purposes. In fact, it was calculated that only 100–200 of the loaded liposomes need to enter a tumor cell to reach the minimum number of boron atoms necessary for the therapy.

Thus, considering the targeting effect toward the nucleus, brought about by cationic lipids and the availability of the sugar moieties on the liposome surface, the potential favorable properties of this loaded vectors were demonstrated.

The authors are indebted to Professor Luigi Panza (Università del Piemonte Orientale, Italy) for the gift of GCOB and LCOB. Thanks are also due to professor Aldo Becciolini, as well as to Dr. Manuela Balzi and Dr. Sauro Porciani (Università di Firenze, Italy), for fruitful discussion on BNCT.

A special acknowledgment is given to Dr. Thomas Zemb (Commissariat à l'Énergie Atomique, Saclay, France) for his valuable input and for providing the opportunity to develop this research project.

REFERENCES

Arleth, L. D., I. S. Posselt, K. Pedersen, D. Mortensen, C. L. Gazeau, and T. N. Zemb. 1997. Small-angle scattering study of tac8: a surfactant with cation complexing potential. *Langmuir*. 13:1887–1896.

Barth, R. F. 2003. A critical assessment of boron neutron capture therapy: an overview. *J. Neuro Onchol*. 62:1–5.

Braun, K., G. Wolber, W. Waldeck, R. Pipkorn, J. Jenne, R. Rastert, V. Ehemann, A. Eisenmenger, H. Corban-Wilhelm, I. Braun, S. Heckl, and J. Debus. 2003. The enhancement of neutron irradiation of HeLa-S cervix carcinoma cells by cell-nucleus-addressed deca-*p*-boronophenylalanine. *Eur. J. Med. Chem.* 38:587–595.

Cantù, L., M. Corti, E. Del Favero, M. Dubois, and T. N. Zemb. 1998. Combined small-angle x-ray and neutron scattering experiments for thickness characterization of ganglioside bilayers. *J. Phys. Chem. B*. 102:5737–5743.

Cevc, G. editor. 1993. Phospholipids Handbook. M. Dekker, New York.

Connolly, M. L. 1994. Adjoint join volumes. *J. Math. Chem*. 15:339–352.

Dupuy, C., X. Auvray, C. Petipas, and R. Anthore. 1998. Influence of structure of polar head on the micellization of lactose-based surfactants. Small-angle x-ray and neutron scattering study. *Langmuir*. 14:91–98.

Endo, Y., T. Iijima, Y. Yamakoshi, H. Fukasawa, C. Miyaura, M. Inada, A. Kubo, and A. Itai. 2001. Potent estrogen agonists based on carborane as a hydrophobic skeletal structure: a new medicinal application of boron clusters. *Chem. Biol.* 8:341–355.

Escher, E., G. Guillemette, O. Leukart, and D. Regoli. 1980. Pharmacological properties of two analogues of angiotensin-II containing carboranylalanine (car). *Eur. J. Pharmacol.* 66:267–272.

Fairchild, R. G., and V. P. Bond. 1985. Current status of ^{10}B-neutron capture therapy: enhancement of tumor dose via beam filtration and dose rate, and the effects of these parameters on minimum boron content: a theoretical evaluation. *Int. J. Rad. Oncol. Biol. Phys.* 11:831–840.

Frisch, M. J., G. W. Trucks, H. B. Schlegel, G. E. Scuseria, M. A. Robb, J. R. Cheeseman, V. G. Zakrzewski, J. A. Montgomery, R. E. Stratmann, J. C. Burant, S. Dapprich, J. M. Millam, A. D. Daniels, K. N. Kudin, M. C. Strain, O. Farkas, J. Tomasi, V. Barone, M. Cossi, R. Cammi, B. Mennucci, C. Pomelli, C. Adamo, S. Clifford, J. Ochterski, G. A. Petersson, P. Y. Ayala, Q. Cui, K. Morokuma, D. K. Malick, A. D. Rabuck, K. Raghavachari, J. B. Foresman, J. Cioslowski, J. V. Ortiz, B. B. Stefanov, G. Liu, A. Liashenko, P. Piskorz, I. Komaromi, R. Gomperts, R. L. Martin, D. J. Fox, T. Keith, M. A. Al-Laham, C. Y. Peng, A. Nanayakkara, C. Gonzalez, M. Challacombe, P. M. W. Gill, B. G. Johnson, W. Chen, M. W. Wong, J. L. Andres, M. Head-Gordon, E. S. Replogle, and J. A. Pople. 1998. Gaussian 98, Rev. A7. Gaussian, Inc., Pittsburgh, PA.

Gabriel, A. 1977. Position-sensitive x-ray detector. *Rev. Sci. Inst.* 48:1303–1306.

Giovenzana, G. B., L. Lay, D. Monti, G. Palmisano, and L. Panza. 1999. Synthesis of carboranyl derivatives of alkynyl glycosides as potential BNCT agents. *Tetrahedron.* 55:14123–14136.

Grillo, I. 2000. Effect of Instrumental Resolution and Polydispersity on Ideal Form Factor in Small Angle Neutron Scattering. ILL Technical Report No. ILL01GR08T.

Hawthorne, M. F., K. Shelly, and R. Wiersma. editors. 2001. Frontiers in Neutron Capture Therapy. Kluwer Academic/Plenum Publishers, New York.

Hayter, J. B., and J. Penfold. 1983. Determination of micelle structure and charge by neutron small-angle scattering. *Colloid Polym. Sci*. 261:1022–1030.

Helfrich, W. 1978. Steric interactions of fluid membranes in multilayer systems. *Z. Naturforsch.* 33:305–315.

Hermansson, K., M. Wojcik, and S. Sjoberg. 1999. O-, m-, and p-carboranes and their anions: ab initio calculations of structures, electron affinities, and acidities. *Inorg. Chem.* 38:6039–6048.

Hughes, D. J., and R. B. Schwartz. 1958. Neutron Cross Sections. The Brookhaven National Laboratory and The U.S. Atomic Energy Commission, Upton, NY.

Irai, M., H. Iwase, T. Hayakawa, M. Koizumi, and H. Takahashi. 2003. Determination of asymmetric structure of ganglioside-DPPC mixed vesicle using SANS, SAXS, and DLS. *Biophys. J.* 85:1600–1610.

Kvítek, J., M. Malečková, K. Baše, J. Plešek, and S. Hermánék. 1975. Detection of boron compounds on chromatography by (n, α) nuclear reaction with thermal neutrons. *J. Chromatogr. A.* 103:385–389.

Larsson, B., J. Crawford, and R. Weinreich. editors. 1997. Advances in Neutron Capture Therapy. Elsevier, Amsterdam, The Netherlands.

Lasic, D. D., and D. Papahadjopoulus. editors. 1998. Medical Applications of Liposomes. Elsevier, Amsterdam, The Netherlands.

Lasic, D. D., H. Strey, M. C. A. Stuart, R. Podgornik, and P. M. Frederik. 1997. Improved DNA: liposome complexes for increased systemic delivery and gene expression. *J. Am. Chem. Soc.* 119:832–833.

Lindner, P., and T. N. Zemb. editors. 2002. Neutron, X-Rays and Light. Scattering Methods Applied to Soft Condensed Matter. Elsevier, Amsterdam, The Netherlands.

MacDonald, R. C., R. I. MacDonald, B. P. M. Menco, K. Takeshta, N. K. Subbarao, and L. Hu. 1991. Small-volume extrusion apparatus for preparation of large, unilamellar vesicles. *Biochim. Biophys. Acta.* 1061: 297–303.

McIntosh, T. J. 1996. Hydration properties of lamellar and non-lamellar phases of phosphatidylcholine and phosphatidylethanolamine. *Chem. Phys. Lipids.* 81:117–131.

Martin, D., J. Jaballas, J. Arias, H. Lee, and T. Onak. 1996. ^{13}C NMR Studies on carboranes and derivatives: experimental/calculational correlations. *J. Am. Chem. Soc.* 118:4405–4410.

Matsumura, Y., and H. Maeda. 1986. A new concept for macromolecular therapeutics in cancer chemotherapy: mechanism of tumoritropic accumulation of proteins and the antitumor agent SMANCS. *Cancer Res.* 46:6387–6392.

Miller, A. D. 1998. Cationic liposomes for gene delivery. *Angew. Chem. Int. Ed. Engl.* 37:1768–1785.

Nagayasu, A., K. Uchiyama, and H. Kiwada. 1999. The size of liposomes: a factor which affects their targeting efficiency to tumors and therapeutic activity of liposomal antitumor drugs. *Adv. Drug Del. Rev.* 40:75–87.

Pedersen, J. S. 1997. Analysis of small-angle scattering data from colloids and polymer solutions: modeling and least-squares fitting. *Adv. Coll. Interf. Sci.* 70:171–210.

Pliška, V., M. Schmidt, and J. L. Fauchère. 1981. Partition coefficients of amino acids and hydrophobic parameters π of their side-chains as measured by thin-layer chromatography. *J. Chromatogr.* 216:79–92.

Porte, G. and J. Appell. 1981. Growth and size distribution of cetylpyridinium bromide micelles in high, ionic strength aqueous solutions. *J. Phys. Chem.* 85:2511–2519.

Radler, J. O., I. Koltover, T. Salditt, and C. R. Safinya. 1997. Structure of DNA-cationic liposome complexes: DNA intercalation in multilamellar membranes in distinct interhelical packing regimes. *Science.* 275:791–792.

Risul, F., M. Dubois and T. N. Zemb. 1998. Phase equilibria and equation of state of a mixed cationic surfactant-glycolipid lamellar system. *Langmuir.* 10:2645–2655.

Robertson, B. W., S. Adenwalla, A. Harken, P. Welsch, J. I. Brand, and P. A. Dowben. 2002. A class of boron-rich solid-state neutron detectors. *Appl. Phys. Lett.* 80:3644–3646.

Ryynänen, P. M., M. Kortesniemi, J. A. Coderre, A. Z. Diaz, P. Hiismäki, and S. E. Savolainen. 2000. Models for estimation of the ^{10}B concentration after BPA-fructose complex infusion in patients during epithermal neutron irradiation in BNCT. *Int. J. Rad. Oncol. Biol. Phys.* 48:1145–1154.

Safinya, C. R. 2001. Structures of lipid-DNA complexes: supramolecular assembly and gene delivery. *Curr. Opin. Struct. Biol.* 11:440–448.

Safran, S. A. 2002. Statistical thermodynamics of soft surfaces. *Surface Science.* 500:127–146.

Shelly, K., D. A. Feakes, M. F. Hawthorne, P. G. Schmidt, T. A. Krisch, and W. F. Bauer. 1992. Model studies directed toward the boron neutron-capture therapy of cancer: boron delivery to murine tumors with liposomes. *Proc. Natl. Acad. Sci. USA.* 89:9039–9043.

Sjöland, K. A., P. Kristiansson, M. Elfman, K. G. Malmqvist, J. Pallon, R. J. Utui, and C. Yang. 1997. Subcellular analysis of boron with a nuclear microprobe. *Nucl. Inst. Meth. Phys. Res. B.* 129:101–105.

Söderman, O., and I. Joanson. 2000. Polyhydroxyl-based surfactants and their physico-chemical properties and applications. *Curr. Op. Coll. Interf. Sci.* 4:391–401.

Soloway, H., W. Tjarks, B. A. Barnum, F. G. Rong, R. F. Barth, I. M. Codogni, and J. G. Wilson. 1998. The chemistry of neutron capture therapy. *Chem. Rev.* 98:1515–1562.

Stradner, A., O. Glatter, and P. A. Schurtemberger. 2000. Hexanol-induced sphere-to-flexible cylinder transition in aqueous alkyl polyglucoside solutions. *Langmuir.* 16:5354–5364.

Szegedi, S., M. Váradi, C. M. Buczkó, M. Várnagi, and T. Sztaricskai. 1990. Determination of boron in glass by neutron transmission method. *J. Radioanal. Nucl. Chem. Lett.* 146:177–184.

Tietze, L. F., and U. Bothe. 1998. Ortho-carboranyl glycosides of glucose, mannose, maltose and lactose for cancer treatment by boron neutron-capture therapy. *Chem. Eur. J.* 4:1179–1183.

Tietze, L. F., U. Bothe, U. Griesbach, M. Nakaichi, T. Hasegawa, H. Nakamura, and Y. Yamamoto. 2001. Ortho-carboranyl glycosides for the treatment of cancer by boron neutron capture therapy. *Bioorg. Med. Chem.* 9:1747–1752.

Türker, L. 2003. The ortho- to metaisomerization of dicarba-closo-dodecaborane. *J. Mol. Struct. Theochem.* 631:75–78.

Valliant, J. F., K. J. Guenther, A. S. King, P. Morel, P. Shaffer, O. O. Sogbein, and K. A. Stephenson. 2002. The medicinal chemistry of carboranes. *Coord. Chem. Rev.* 232:173–230.

Wiener, M. C., and S. H. White. 1991. Fluid bilayer structure determination by the combined use of x-ray and neutron diffraction. I. Fluid bilayer models and the limits of resolution. *Biophys. J.* 59:162–185.

Yamamoto, K., and Y. Endo. 2001. Utility of boron clusters for drug design. Hansch-Fujita hydrophobic parameters π of dicarba-closo-dodecaboranyl groups. *Bioorg. Med. Chem. Lett.* 11:2389–2392.

Zemb, T. N., O. Taché, F. Né, and O. Spalla. 2003. Sensitivity of a small angle x-ray scattering camera with pinhole collimation using separated optical elements. *Rev. Sci. Inst.* 4:2456–2462.

Zhang, R., P. A. Marone, P. Thiyagarajan, and D. M. Tiede. 1999. Structure and molecular fluctuations of n-alkyl-β-D-glucopyranoside micelles determined by x-ray and neutron scattering. *Langmuir.* 15: 7510–7519.